Complex collective states in a one-dimensional two-atom system

Gonzalo Ordonez and Sungyun Kim
Center for Studies in Statistical Mechanics and Complex Systems, The University of Texas at Austin, Austin, Texas 78712, USA
(Received 11 December 2003; published 3 September 2004)

We consider a pair of identical two-level atoms interacting with a scalar field in one dimension, separated by a distance x_{21}. We obtain collective decaying states, belonging to a complex spectral representation of the Hamiltonian. The imaginary parts of the eigenvalues give the decay rates, and the real parts give the average energy of the collective states. In one dimension there is strong interference between the fields emitted by the atoms, producing cooperative effects even when the atoms are far apart. The decay rates and the energy oscillate with the distance x_{21}. Depending on x_{21}, the decay rates will either decrease, vanish, or increase as compared with the one-atom decay rate. We have sub- and superradiance at periodic intervals. Our model may be used to study two-cavity electron waveguides. The vanishing of the collective decay rates then suggests the possibility of obtaining stable configurations, where an electron is trapped inside the two cavities.

DOI: 10.1103/PhysRevA.70.032702 PACS number(s): 32.80.−t, 03.65.−w, 73.63.−b

I. INTRODUCTION

Systems of interacting atoms form collective states where the atoms behave differently from isolated ones [1,2]. For atoms in their ground states the collective effects are relatively small. They produce the van der Waals or Casimir-Polder forces between atoms [3], associated with the cloud of virtual photons surrounding the atoms.

When the atoms are in excited states they can exchange real photons originated by spontaneous emission. Depending on the situation, the real photons can give strong collective effects, altering the forces between atoms and also their rate of spontaneous emission [1,4,5]. For example, for identical atoms in three dimensions separated by small distances, the decay rate will essentially double or vanish, depending on whether the initial state is symmetric or antisymmetric with respect to exchange of atoms [4,6]. We have "superradiance" or "subradiance," respectively. If the atoms are not identical [7], or if the distance between the atoms is larger than their characteristic wavelengths, the effects become much smaller [4].

Previous studies on two atoms (see, e.g., Refs. [1–10]) have mainly focused on three-dimensional (3D) systems. In this paper we will study a model of two atoms in one dimension. Our motivation is to understand how the field emitted by an excited atom (real photon) influences another atom, using an exactly solvable model.

In 1D, the effects of real photon exchange are expected to be large, as compared with higher-dimensional systems, because interference effects are stronger. In 1D the real photons emitted by a single atom are associated with a field growing exponentially with the distance from the atom, up to the light cone [11]. The growth in space is related to the exponential decay of the atom in time. As we will show, this exponential field produces significant effects on the collective states that, in contrast to 3D systems, are not limited to the near zone of the atoms.

The exponential component of the emitted field can be separated through complex spectral representations of the Hamiltonian [12–15], including complex eigenvalues and eigenstates. The complex eigenvalues are obtained through the solutions of integral equations for the Green's function poles. They give the decay rates and average energies of the complex eigenstates.

Since the Hamiltonian is a Hermitian operator, it can have only complex eigenstates outside the Hilbert space. In one-atom systems the non-Hilbertian nature of these states is manifested in their field intensity, which includes the exponentially growing factor mentioned above.[1]

For the two-atom model we consider here, the exponentially growing field itself appears in the equations for the Green's function poles. By solving these equations we obtain explicit forms of the complex collective states and their decay rates.

Our main result is that the decay rates of the collective states oscillate with the distance between the atoms, even for large separations. For distances that are roughly integer multiples of the atom wavelength, the collective decay rates vanish, leading to collective stable states. Our results are verified by numerical simulations. In contrast to Dicke's states [1], both symmetric and antisymmetric states of the two atoms can become subradiant and superradiant as the distance between the two atoms is varied.

From a physical point of view, the present study is of interest because our model can be mapped to electron waveguides consisting of two cavities connected by a lead [17,18]. As discussed in Sec. VII, our result shows the existence of approximate bound states, due to the resonance excitation transfer between cavities. These bound states may be used as electron traps.

The paper is organized as follows. In Sec. II we briefly discuss the complex spectral representation of the Hamiltonian for a one-atom system. In Sec. III we introduce our two-atom model and its complex collective eigenstates. In

[1]Including the complete set of eigenstates in the complex representation of the Hamiltonian, the exponential field outside the light cone is canceled by renormalized field states. This is consistent with causality [11]. One can introduce complex states that are truncated outside the light cone, using distributions dependent on the test functions or observables. These are considered in Ref. [16].

Secs. IV and V we discuss the emergence of the collective states and the bouncing of photons between the atoms. In Sec. VI we consider the decay rate and average energy of the collective states as a function of the distance between the atoms. We discuss superradiance and subradiance, including the stable collective states mentioned above. We also give a heuristic discussion of the force between the atoms. In Sec. VII we discuss the mapping of our model to a two-cavity electron waveguide, and, within some approximations, show that this system allows stable collective states.

II. ONE-ATOM SYSTEM

In order to introduce the complex spectral representation of the Hamiltonian, we consider first a single two-level atom interacting with a field in one-dimensional space. This is the Friedrichs-Lee model in one dimension. We briefly review the main results. More details can be found in Ref. [15].

For convenience hereafter we use units where $c=\hbar=1$. We write the Hamiltonian as

$$H' = \omega_0 H, \tag{1}$$

where ω_0 is a characteristic atomic frequency and H is a dimensionless Hamiltonian. For this dimensionless Hamiltonian, the dynamical variables time, space, energy, and momentum are dimensionless too.

We have

$$H = H_0 + \lambda V = \omega_1 |1\rangle\langle 1| + \sum_k \omega_k |k\rangle\langle k| + \lambda \sum_k V_k (|k\rangle\langle 1| + |1\rangle\langle k|). \tag{2}$$

The state $|1\rangle$ represents the bare atom in its excited level with no field present, while the state $|k\rangle$ represents a bare field mode ("photon") of momentum k together with the atom in its ground state.

The energy of the ground state is chosen to be zero; ω_1 is the bare energy of the excited level and $\omega_k \equiv |k|$ is the photon energy. The coupling constant $\lambda \ll 1$ is dimensionless. For the field modes we use box normalization. We put the system in a "box" of size L and use periodic boundary conditions. For L finite the momenta k are discrete. Hereafter we will consider the limit $L \to \infty$. In this limit the field modes become continuous, i.e.,

$$\frac{2\pi}{L} \sum_k \to \int dk. \tag{3}$$

We have $\langle a|b\rangle = \delta_{a,b}$ (Kroenecker delta). In the limit $L \to \infty$,

$$\frac{L}{2\pi} \delta_{k,k'} \to \delta(k-k'). \tag{4}$$

The interaction term is obtained through the dipole approximation as well as the rotating-wave approximation. The potential V_k is of order $L^{-1/2}$. For convenience we write

$$V_k = (2\pi/L)^{1/2} v_k, \tag{5}$$

where v_k is of order 1 in the continuous spectrum limit $L \to \infty$. As a specific example we will assume that [19,20]

$$v_k = v(\omega_k) = \frac{\omega_k^{1/2}}{[1 + (\omega_k/\omega_M)^2]^n} \tag{6}$$

with $n=1$. The constant ω_M^{-1} determines the range of the interaction. We shall assume that the interaction is of short range, i.e., $\omega_M \gg \omega_1$.

The state $|1\rangle$ is unstable if

$$\omega_1 > \int_{-\infty}^{\infty} dk \frac{\lambda^2 v_k^2}{\omega_k}. \tag{7}$$

Otherwise, it is stable [21]. Hereafter we will consider the unstable case.

In the unstable case one can construct renormalized field eigenstates that diagonalize the Hamiltonian as

$$H = \sum_k |\tilde{\phi}_k^{\pm}\rangle \omega_k \langle \tilde{\phi}_k^{\pm}|, \tag{8}$$

where

$$\lim_{\lambda \to 0} |\tilde{\phi}_k^{\pm}\rangle = |k\rangle, \tag{9}$$

and hereafter we use the summation over field modes in the sense of Eq. (3). The index $\pm$ refers to either "in" or "out" scattering eigenstates.

The explicit form of the eigenstates is given by [15]

$$|\tilde{\phi}_k^{\pm}\rangle = |k\rangle + \frac{\lambda V_k}{\eta^{\pm}(\omega_k)} \left[|1\rangle + \sum_l \frac{\lambda V_l}{\omega_k - \omega_l \pm i\epsilon} |l\rangle \right], \tag{10}$$

where ϵ is an infinitesimal positive number. The limit $\epsilon \to 0$ is taken after the limit $L \to \infty$. In Eq. (10),

$$\eta^{\pm}(z) \equiv z - \omega_1 - \sum_{k'} \frac{\lambda^2 V_{k'}^2}{(z-\omega_{k'})^{\pm}} = z - \omega_1 - 2\int_0^{\infty} dk' \frac{\lambda^2 v_{k'}^2}{(z-k')^{\pm}} \tag{11}$$

is the inverse of the Green's function. The + (or −) superscript in Eq. (11) indicates analytic continuation from the upper (or lower) half plane of z [15]. Using the complex delta function δ_C [12] we can write

$$\frac{1}{(z-k')^{\pm}} = \begin{cases} (z-k')^{-1}, & \pm \mathrm{Im}\, z > 0, \\ (z-k')^{-1} \mp 2\pi i \delta_C(k'-z), & \pm \mathrm{Im}\, z < 0. \end{cases} \tag{12}$$

When $z=\omega$ is real, we have

$$\eta^{\pm}(\omega) \equiv \omega - \omega_1 - 2\int_0^{\infty} dk' \frac{\lambda^2 v_{k'}^2}{\omega - k' \pm i\epsilon}. \tag{13}$$

With the form factor in Eq. (6), the Green's function has one pole z_1 in the lower half plane, i.e., $\eta^+(z_1)=0$,

$$z_1 \equiv \tilde{\omega}_1 - i\gamma_1, \tag{14}$$

which reduces to ω_1 when $\lambda \to 0$. The negative imaginary part $-i\gamma_1$ describes decay for $t>0$.[2] The real part $\tilde{\omega}_1$ gives the shifted average energy of the excited state. For the other branch we have $\eta^-(z_1^*)=0$, with z_1^* describing decay for $t<0$.

Note that in the representation (8) the decay rate and shifted energy of the excited state do not appear in the spectrum. One can incorporate z_1 (or z_1^*) into the spectrum by extracting the residue of Eq. (8) at the pole $\omega_k=z_1$ (or z_1^*). This gives the complex spectral decompositions [12–15]

$$H = |\phi_1\rangle z_1 \langle\tilde{\phi}_1| + \sum_k |\phi_k^+\rangle \omega_k \langle\tilde{\phi}_k^+| = |\tilde{\phi}_1\rangle z_1^* \langle\phi_1| + \sum_k |\phi_k^-\rangle \omega_k \langle\tilde{\phi}_k^-|. \tag{15}$$

The state $|\phi_1\rangle$ and its dual $\langle\tilde{\phi}_1|$ are complex eigenstates of H. Their explicit forms are [15]

$$|\phi_1\rangle = N_1^{1/2}\left[|1\rangle + \sum_k |k\rangle \frac{\lambda V_k}{(z_1-\omega_k)^+}\right], \tag{16}$$

$$|\tilde{\phi}_1\rangle = [N_1^*]^{1/2}\left[|1\rangle + \sum_k |k\rangle \frac{\lambda V_k}{(z_1^*-\omega_k)^-}\right],$$

$$N_1 = \left[1 + \sum_k \lambda^2 V_k^2/[(z_1-\omega_k)^+]^2\right]^{-1}. \tag{17}$$

The state $|\phi_k^+\rangle$ has the same form as the state $|\tilde{\phi}_k^+\rangle$ with the replacement

$$\frac{1}{\eta^+(\omega_k)} \Rightarrow \frac{1}{\eta^+(\omega_k)} \frac{\omega_k - z_1}{(\omega_k - z_1)^+}, \tag{18}$$

and similarly the state $|\phi_k^-\rangle$ has the same form as the state $|\tilde{\phi}_k^-\rangle$ with the complex conjugate replacement.

The states in Eq. (15) form a biorthormal set, with the relations

$$\langle\tilde{\phi}_1|\phi_1\rangle = 1, \quad \langle\tilde{\phi}_k^+|\phi_1\rangle = 0,$$

$$\langle\tilde{\phi}_k^+|\phi_{k'}^+\rangle = \delta_{k,k'} \tag{19}$$

and their complex conjugate relations.

III. TWO-ATOM SYSTEM

In this section we discuss the complex spectral representation of a one-dimensional, two-atom system with dimensionless Hamiltonian

$$H = \omega_1|1\rangle\langle 1| + \omega_2|2\rangle\langle 2| + \sum_k \omega_k|k\rangle\langle k| + \sum_k \lambda_1(V_{1k}|1\rangle\langle k| + V_{1k}^{c.c}|k\rangle\langle 1|) + \sum_k \lambda_2(V_{2k}|2\rangle\langle k| + V_{2k}^{c.c}|k\rangle\langle 2|). \tag{20}$$

The state $|1\rangle$ represents atom 1 in its excited state, while atom 2 is in the ground state and no field is present. Conversely, the state $|2\rangle$ represents atom 2 in its excited state, while atom 1 is in the ground state and no field is present. The state $|k\rangle$ represents a field mode k with both atom 1 and atom 2 in their ground states. We denote the location of the atoms 1 and 2 by x_1 and x_2, respectively. We will first assume that the two atoms are at fixed positions, so that the distance between them

$$x_{21} = |x_2 - x_1| \tag{21}$$

is fixed. This can happen if the atoms are heavy.

We will consider the case where the two atoms are identical,

$$\lambda_1 = \lambda_2 = \lambda,$$

$$\omega_1 = \omega_2, \tag{22}$$

and the potentials V_{1k} and V_{2k} have the forms

$$V_{1k} = V_k e^{ikx_1}, \quad V_{2k} = V_k e^{ikx_2}. \tag{23}$$

For V_k we use the potential in Eq. (6). We introduce the symmetric and antisymmetric states

$$|s\rangle = \frac{|1\rangle + |2\rangle}{\sqrt{2}}, \quad |a\rangle = \frac{|1\rangle - |2\rangle}{\sqrt{2}}, \tag{24}$$

which are degenerate eigenstates of the unperturbed Hamiltonian $H_0=H(\lambda=0)$, as

$$H_0|j\rangle = \omega_j|j\rangle, \quad j = s,a, \tag{25}$$

$$\omega_s = \omega_a = \omega_1. \tag{26}$$

We will use the notation

$$\sigma_j \equiv \begin{cases} 1 & \text{for } j=s, \\ -1 & \text{for } j=a, \end{cases} \tag{27}$$

With this notation we have $|j\rangle=(|1\rangle+\sigma_j|2\rangle)/\sqrt{2}$.

As for the one-atom system, we can diagonalize the Hamiltonian as

$$H = \sum_k |\tilde{F}_k^\pm\rangle \omega_k \langle\tilde{F}_k^\pm|, \tag{28}$$

where

$$|\tilde{F}_k^\pm\rangle = |k\rangle + \beta_{sk}^\pm|s\rangle + \beta_{ak}^\pm|a\rangle + \sum_{k'} \beta_{k'k}^\pm|k'\rangle \tag{29}$$

and

$$\beta_{jk}^\pm = \frac{1}{\sqrt{2}} \frac{\lambda V_k}{\eta_j^\pm(\omega_k)} (e^{ikx_1} + \sigma_j e^{ikx_2}), \tag{30}$$

$$\beta_{k'k}^\pm = \frac{1}{\sqrt{2}} \frac{\lambda V_{k'}}{\omega_k - \omega_{k'} \pm i\epsilon} \sum_{j=s,a} \beta_{jk}^\pm (e^{-ik'x_1} + \sigma_j e^{-ik'x_2}), \tag{31}$$

[2]There are other poles associated with the potential v_k. We will not extract them in the complex representation of H, as they give short-time effects vanishing after a time $t \propto \omega_M^{-1}$.

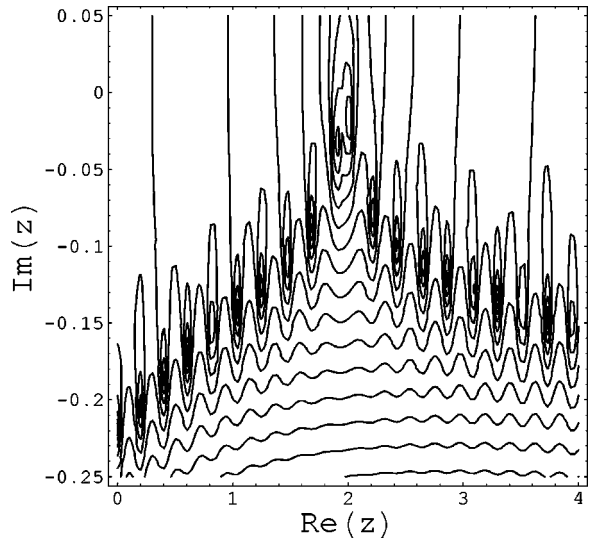

FIG. 1. Contour plot of $\ln[1/|\eta_s^+(z)|]$. The contours concentrate around the poles $z_{s,n}$ of the Green's function. The uppermost pole is z_s. The complex frequency z is dimensionless. The contours correspond to the values $-3.5,-3.0,\ldots,3,3.5$ of $\ln[1/|\eta_s^+(z)|]$. Parameters are $x_{21}=29.025$, $\omega_1=2$, $\lambda=0.05$, $\omega_M=5$.

$$\eta_j^{\pm}(z) = z - \omega_1 - 2\int_0^{\infty} dk' \frac{\lambda^2 v_{k'}^2}{(z-k')^{\pm}}[1+\sigma_j \cos(k' x_{21})]. \tag{32}$$

Following a procedure similar to one found in Ref. [15], one can show that the new diagonalized states $|\tilde{F}_k^{\pm}\rangle$ satisfy the orthogonality and completeness relations

$$\sum_k |\tilde{F}_k^{\pm}\rangle\langle\tilde{F}_k^{\pm}| = |1\rangle\langle 1| + |2\rangle\langle 2| + \sum_k |k\rangle\langle k|, \tag{33}$$

$$\langle\tilde{F}_k^{+}|\tilde{F}_{k'}^{+}\rangle = \langle\tilde{F}_k^{-}|\tilde{F}_{k'}^{-}\rangle = \delta_{k,k'}. \tag{34}$$

The Green's function $[\eta_j^+(z)]^{-1}$ has poles in the lower half plane, and conversely $[\eta_j^-(z)]^{-1}$ has poles in the upper half plane. From now on we discuss only the + branch with poles on the lower half plane.

A new feature with respect to the one-atom system is that due to the cosine term in Eq. (32) there are infinitely many poles of the Green's function, as shown in Fig. 1. We label the poles as

$$z_{j,n} = \tilde{\omega}_{j,n} - i\gamma_{j,n}, \tag{35}$$

where n is an integer.[3]

The poles $z_{j,n}$ are solutions of the equation

$$\eta_j^+(z_{j,n}) = 0. \tag{36}$$

In the following we discuss this equation and its solutions.

From Eqs. (12) and (32) we obtain

$$z_{j,n} = \omega_1 + 2\int_0^{\infty} dk' \frac{\lambda^2 v_{k'}^2}{z_{j,n}-k'}[1+\sigma_j\cos(k' x_{21})] - 4\pi i\lambda^2[v_{z_{j,n}}]^2[1+\sigma_j\cos(z_{j,n}x_{21})]. \tag{37}$$

Assuming weak coupling and taking only the pole contribution in the k' integral we obtain the set of equations

$$\tilde{\omega}_{j,n} \approx \omega_1 + 2\pi[\lambda v(\tilde{\omega}_{j,n})]^2\sigma_j e^{\gamma_{j,n}x_{21}}\sin(\tilde{\omega}_{j,n}x_{21}), \tag{38}$$

$$\tilde{\gamma}_{j,n} \approx 2\pi[\lambda v(\tilde{\omega}_{j,n})]^2[1+\sigma_j e^{\gamma_{j,n}x_{21}}\cos(\tilde{\omega}_{j,n}x_{21})]. \tag{39}$$

Note the factor $\exp(\gamma_{j,n}x_{21})$, which grows exponentially with the distance x_{21} between the atoms.

In Fig. 1, the pole of $[\eta_s^+(z)]^{-1}$ with real part closest to the unperturbed frequency ω_1 is also closest to the real axis. We call this pole $z_s \equiv z_{s,0}$. Similarly, for $[\eta_a^+(z)]^{-1}$ we denote the pole closest to ω_1 as $z_a \equiv z_{a,0}$. Both these poles are obtained by a perturbation expansion around $\lambda=0$. We have

$$z_{j,0} = z_j \to \omega_1 \quad \text{as } \lambda \to 0. \tag{40}$$

If x_{21} is not too large ($x_{21} \sim \gamma_1^{-1}$ or smaller), one can show by substitution into Eqs. (38) and (39) that the poles $z_{j,n}$ are given by

$$z_{j,n} = \begin{cases} z_j + 2n\pi/x_{21} + \delta z_{j,n} & \text{for } \sigma_j n > 0, \\ z_j + (2n+\sigma_j)\pi/x_{21} + \delta z_{j,n} & \text{for } \sigma_j n < 0, \end{cases} \tag{41}$$

where $\delta z_{j,n}$ is an $O(\lambda^2)$ correction. The approximate value $\mathrm{Re}(z_{j,n}-z_j)$ predicted by this equation agrees with Fig. 1 (for $j=s$) and a similar figure for $j=a$, which we omit.

We write the poles z_j as

$$z_j = \tilde{\omega}_j - i\gamma_j. \tag{42}$$

The poles z_j, having the smallest decay rates γ_j, will give a dominant contribution to the time evolution after a few bounces of the field between the atoms, when the complex collective states defined in Eq. (43) emerge.

As in the one-atom system we can obtain complex eigenstates $|\phi_j\rangle$ of the total Hamiltonian, such that

$$H|\phi_j\rangle = z_j|\phi_j\rangle. \tag{43}$$

Their explicit forms are given by

$$|\phi_j\rangle = N_j^{1/2}\left[|j\rangle + \sum_k \frac{2^{-1/2}\lambda V_k}{(z_j-\omega_k)^+}(e^{-ikx_1}+\sigma_j e^{-ikx_2})|k\rangle\right], \tag{44}$$

where

$$N_j = \left[1 + \sum_k \frac{\lambda^2 V_k^2}{[(z_j-\omega_k)^+]^2}(1+\sigma_j\cos kx_{21})\right]^{-1}. \tag{45}$$

For these states we have $|\phi_j\rangle \to |j\rangle$ as $\lambda \to 0$.

The dual states satisfying $\langle\tilde{\phi}_j|H = z_j\langle\tilde{\phi}_j|$ are given by

$$\langle\tilde{\phi}_j| = N_j^{1/2}\left[\langle j| + \sum_k \frac{2^{-1/2}\lambda V_k}{(z_j-\omega_k)^+}(e^{ikx_1}+\sigma_j e^{ikx_2})\langle k|\right]. \tag{46}$$

As in the one-atom case, we have the complex spectral representation

[3] As in the one-atom system there are in addition poles associated with the potential.

$$H = \sum_{j=s,a} |\phi_j\rangle z_j \langle\tilde{\phi}_j| + \sum_k |F_k^+\rangle \omega_k \langle\tilde{F}_k^+|, \tag{47}$$

where $|F_k^+\rangle$ has the same form as the state $|\tilde{F}_k^+\rangle$ with the replacement

$$\frac{1}{\eta_j^+(\omega_k)} \Rightarrow \frac{1}{\eta_j^+(\omega_k)} \frac{\omega_k - z_j}{(\omega_k - z_j)^+}. \tag{48}$$

We have as well the complex conjugate representation, taking the complex conjugates of Eqs. (47) and (48).

IV. EMERGENCE OF THE COMPLEX COLLECTIVE STATES

The time evolution of the two-atom system can be solved by using Eq. (28) or Eq. (47). As an example we assume the atoms are initially in the symmetric state $|s\rangle$ and the initial field is zero (similar calculations can be done if the initial state is $|a\rangle$). We will calculate the survival probability of state $|1\rangle$,

$$P_1(t) = |\langle 1|e^{-iHt}|s\rangle|^2. \tag{49}$$

Before we go into details, we can guess the behavior the system will show. Since the initial state is symmetric, the following discussion also applies with atoms 1 and 2 exchanged. Say atom 1 is to the left of atom 2. At the beginning, atom 1 decays and emits a field. Half of this field will be radiated away to the left, while the other half will reach and excite atom 2. Atom 2 will then decay and emit its own field, part of which will be radiated away to the right, the rest going to the left, back toward atom 1. Continuing this process, we see that energy will bounce back and forth between the two atoms. As time passes, this energy will decrease due to the outgoing radiation. Eventually both atoms will decay to the ground state. Noting that the time it takes for the field of one atom to reach the other atom is $t = x_{21}$ (with $c = 1$) we conclude that, as it decreases, the survival probability should oscillate with period x_{21}.

This behavior is shown in Fig. 2. This was obtained through a numerical solution of Schrödinger's equation. The field was discretized into 2501 modes. The eigenvalues and eigenfunctions of the Hamiltonian matrix were obtained using tridiagonalization and the "QL" method based on the decomposition $H = QL$, where Q is an orthogonal matrix and L is a lower triangular matrix [22]. This allowed us to calculate explicitly the operator $\exp(-iHt)$. For this and the subsequent numerical plots we used the following parameters: $\omega_1 = 2$, $\lambda = 0.05$, $\omega_M = 5$. Other parameters are indicated in each figure.

In order to calculate the survival probability analytically, we start with Eq. (28), to obtain

$$P_1(t) = |\langle 1|e^{-iHt} \sum_k |\tilde{F}_k^+\rangle \langle\tilde{F}_k^+|s\rangle|^2 = \left| \sum_k e^{-i\omega_k t} \langle 1|\tilde{F}_k^+\rangle \langle\tilde{F}_k^+|s\rangle \right|^2$$
$$= \frac{1}{2} \left| \sum_k e^{-i\omega_k t} \frac{\lambda^2 V_k^2}{|\eta_s^+(\omega_k)|^2} (1 + \cos k x_{21}) \right|^2, \tag{50}$$

where we used the fact that odd functions of k vanish under the summation. For later use we define the amplitude in Eq. (50) as

$$\mathcal{A}(t) \equiv \sum_k e^{-i\omega_k t} \frac{\lambda^2 V_k^2}{|\eta_s^+(\omega_k)|^2} (1 + \cos k x_{21}). \tag{51}$$

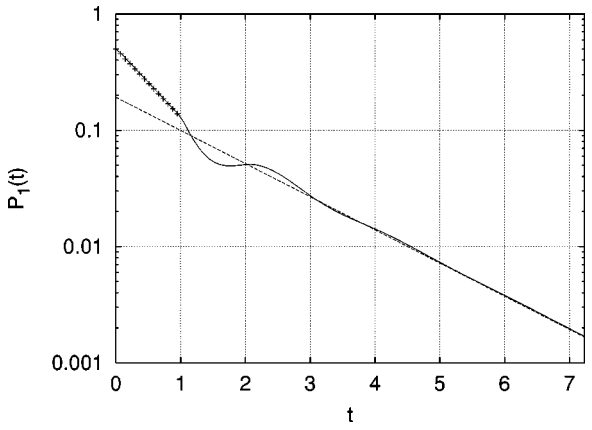

FIG. 2. Logarithmic plot of the survival probability $P_1(t)$ (solid line) and complex collective-state component $P_{1,zs}(t)$ (dashed line). Time t has been scaled to units of $x_{21} = 29.025$. The crosses indicate the decay rate $2\gamma_{s1}$, $\gamma_{s1} = 0.0233$, between $t = 0$ and $t = 1$ (see Sec. V). Parameters are $\omega_1 = 2$, $\lambda = 0.05$, $\omega_M = 5$, and $L = 500$.

The dominant contribution to $P_1(t)$ will come from the poles of the Green's function shown in Fig. 1. The different pole contributions should add up to give the bounces seen in Fig. 2. But rather than computing all the pole contributions, we will follow an easier method in Sec. V.

Here we will focus on the pole z_s. As mentioned before, this will give the dominant contribution after some bounces, since it gives the slowest decay rate. It is this pole contribution that is extracted in the representation (47). Using this representation and noting that $\langle\tilde{\phi}_a|s\rangle = 0$, we have

$$P_1(t) = \left| \langle 1|\phi_s\rangle e^{-iz_s t} \langle\tilde{\phi}_s|s\rangle + \sum_k \langle 1|F_k^+\rangle e^{-i\omega_k t} \langle\tilde{F}_k^+|s\rangle \right|^2. \tag{52}$$

The second term contains contributions from poles other than z_s of the Green's function $[\eta_s^+(\omega)]^{-1}$ as well as contributions coming from the branch cut of this function. Neglecting all these contributions we obtain

$$P_1(t) \approx P_{1,zs}(t) \equiv |\langle 1|\phi_s\rangle e^{-iz_s t} \langle\tilde{\phi}_s|s\rangle|^2. \tag{53}$$

This is represented by the dashed line in Fig. 2. After a few bounces the initial state $|s\rangle$ reaches the collective state $|\phi_s\rangle$.

We turn to the time evolution of the field. Defining the state

$$|\psi(x)\rangle = \sum_k \frac{1}{(2\omega_k L)^{1/2}} e^{-ikx} |k\rangle, \tag{54}$$

the intensity of the field in space-time can be written as

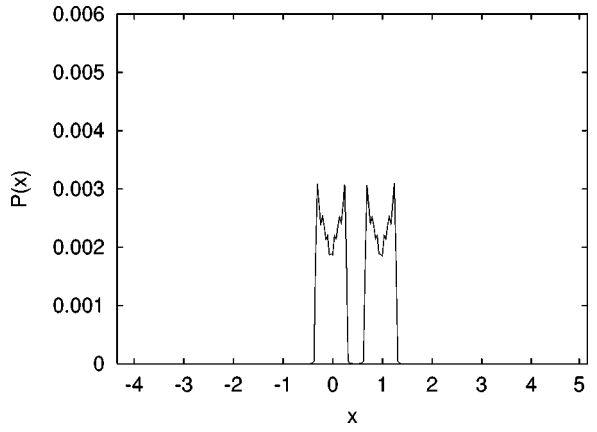

FIG. 3. Field intensity $P(x,t)$ for $t=0.32x_{21}$. Space coordinate x has been scaled to units of $x_{21}=29.025$ and $P(x,t)$ is dimensionless. The atoms are located at $x_1=0$ and $x_2=1$. The parameters are the same as in Fig. 2.

$$P(x,t)=\left|\langle\psi(x)|e^{-iHt}|s\rangle\right|^2. \tag{55}$$

Again we calculated this using the numerical solution of Schrödinger's equation. The intensity of the field is plotted in Figs. 3–5 for different times. At the beginning, both atoms emit their fields spontaneously. Each field has an exponentially growing envelope (plus corrections due to the initial dressing processes [11]), which stops at the light cone $|x-x_i|=t$ (Fig. 3).

After each emitted field reaches the neighbor atom, absorption and reemission occur. The two atoms exchange energy, and the field $P(x,t)$ around the atoms starts to approach the field intensity due to the collective state given by

$$P_{zs}(x,t)=\left|\langle\psi(x)|\phi_s\rangle\exp(-iz_st)\langle\phi_s|s\rangle\right|^2 \tag{56}$$

(see Fig. 4). The collective state decays exponentially (Fig. 5).

In summary, the atoms emit a field growing exponentially with the distance from them, within their light cones. After the field emitted from each atom reaches the other one, the collective state with complex energy z_j emerges.

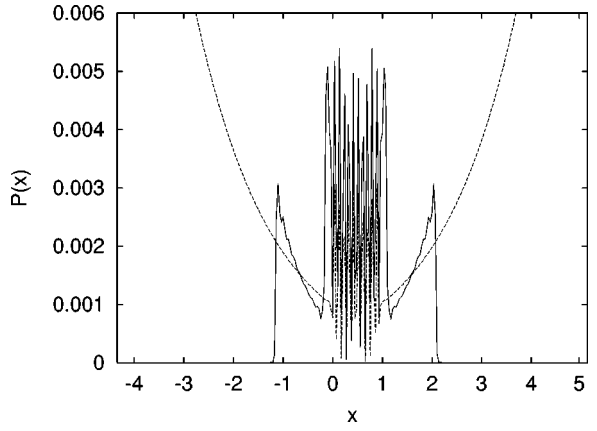

FIG. 4. Field intensity $P(x,t)$ for $t=1.12x_{21}$ (solid line) and the complex collective-state component $P_{zs}(x,t)$ (dashed line). Space coordinate x is in units of $x_{21}=29.025$ and $P(x,t)$ is dimensionless. Parameters are the same as in Fig. 2.

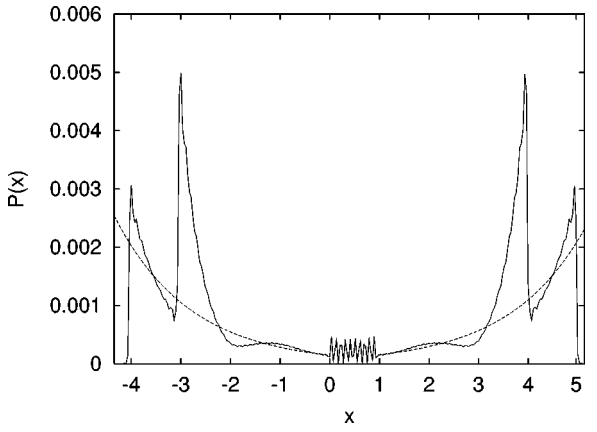

FIG. 5. Field intensity $P(x,t)$ for $t=4.02x_{21}$ (solid line) and the complex collective-state component $P_{zs}(x,t)$ (dashed line). Space coordinate x is in units of $x_{21}=29.025$ and $P(x,t)$ is dimensionless. The outer smaller peaks of $P(x,t)$ come from the initial one-atom emission. The inner, larger peaks come from the emission after the first exchange of energy between the atoms. $P(x,t)$ asymptotically approaches $P_{zs}(x,t)$ as x approaches the atoms. They coincide in the region between the atoms (between $x=0$ and $x=1$). Parameters are the same as in Fig. 2.

As we discuss now, the exponential field has a strong influence on z_j. The field amplitude associated with the collective states is given by $\langle k|\phi_j\rangle$. This amplitude in turn determines z_j through its interaction with the atoms. We have

$$z_j=\omega_1+\frac{1}{\sqrt{2N_j}}\sum_k \lambda V_k[e^{ikx_1}+\sigma_j e^{ikx_2}]\langle k|\phi_j\rangle, \tag{57}$$

where we used Eqs. (43), (44), and (32), with $\omega=z_j$. Since $\langle k|\phi_j\rangle$ are functions of z_j, this is a self-consistent relation. From Eqs. (38) and (39) for $z_{j,0}=z_j$, we get

$$\langle k|\phi_j\rangle\propto\exp(\gamma_j x_{21}). \tag{58}$$

Due to the exponential nature of this factor, the pole z_j may deviate substantially from the one-atom pole z_1.

In spite of the exponential factor, for increasing x_{21} Eqs. (38) and (39) can still have solutions since γ_j decreases at least as

$$\gamma_j\sim x_{21}^{-1} \tag{59}$$

for large x_{21}. This decrease of γ_j with increasing x_{21} is seen in Fig. 6.

V. BOUNCES

In this section we describe the energy bounces between the atoms, seen in the survival probability of $P_1(t)$ of atom 1 (since we are assuming the initial state is symmetric, the survival probability of atom 2 is the same). We discuss how repeated bounces lead to the appearance of collective states. We obtain a piecewise expression for the survival probability, which gives a connection with the results presented in Refs. [5,6].

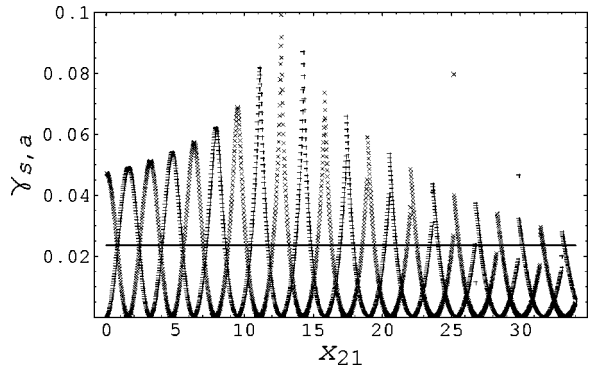

FIG. 6. The decay rates γ_s (×) and γ_a (+) oscillating as a function of x_{21}. The solid line is the one-atom decay rate $\gamma_1=0.0235$. γ_s vanishes for distances close to $(2n-1)\pi/\tilde{\omega}_1$, and γ_a for distances close to $2n\pi/\tilde{\omega}_1$ with n integer. For $x_{21}=12.7\approx 8\pi/\tilde{\omega}_1$, γ_a vanishes, while γ_s takes its maximum value. For large x_{21} the decay rates decrease. Both x_{21} and $\gamma_{s,a}$ are dimensionless.

As shown in Fig. 2, the decay rate of $P_1(t)$ changes abruptly at $t=x_{21}$. For $t>x_{21}$ the decay rate quickly approaches the collective decay rate γ_s. The wiggling of the decay rate shows the absorption and reemission of the fields, or in other words the energy bounces. For $0<t<x_{21}$ the decay rate should be close to the one-particle decay rate.

To analyze the energy bounces and the decay for $0<t<x_{21}$ we first note that

$$\eta_s^+(k)-\eta_s^-(k)=4\pi i\lambda^2 v_k^2(1+\cos kx_{21}). \tag{60}$$

Hence in Eq. (51) we can write

$$\mathcal{A}(t)=2\int_0^\infty dk e^{-i\omega_k t}\frac{\lambda^2 v_k^2}{|\eta_s^+(k)|^2}(1+\cos kx_{21})$$
$$=\frac{1}{2\pi i}\int_0^\infty dk\left(\frac{1}{\eta_s^-(k)}-\frac{1}{\eta_s^+(k)}\right)e^{-ikt}. \tag{61}$$

Since e^{-ikt} vanishes in the lower infinite semicircle of the complex k plane for $t>0$, we can take the pole contributions, extending the k integration from $-\infty$ to ∞ and closing the contour with this semicircle. Only $[\eta_s^+(k)]^{-1}$ has poles in the lower half plane. We write $\eta_s^+(k)$ as

$$\eta_s^+(k)=k-\omega_1-2\int_0^\infty dk'\frac{\lambda^2 v_{k'}^2(1+\cos k'x_{21})}{k-k'+i\epsilon}=\eta_{s1}^+(k)-\Delta(k), \tag{62}$$

where $\eta_{s1}^+(k)$ is defined by

$$\eta_{s1}^+(k)=k-\omega_1-2\int_0^\infty dk'\frac{\lambda^2 v_{k'}^2}{k-k'+i\epsilon}\left(1+\frac{1}{2}e^{-ik'x_{21}}\right)$$
$$-\int_0^\infty dk'\frac{\lambda^2 v_{k'}^2 e^{-ik'x_{21}}}{k-k'-i\epsilon} \tag{63}$$

and

$$\Delta(k)=-2\pi i\lambda^2 v_k^2 e^{ikx_{21}}. \tag{64}$$

The function $[\eta_{s1}^+(k)]^{-1}$ has one pole in the lower half plane that reduces to ω_1 when $\lambda\to 0$. Let this pole be

$$z_{s1}=\tilde{\omega}_{s1}-i\gamma_{s1}. \tag{65}$$

This is essentially the pole of the one-atom Green's function, modified by the overlap of the atomic clouds at the distance x_{21}. For $x_{21}\gg\omega_1^{-1}$ we have

$$z_{s1}\approx z_1. \tag{66}$$

We expand $1/\eta_s^+(k)$ as

$$\frac{1}{\eta_s^+(k)}=\frac{1}{\eta_{s1}^+(k)-\Delta(k)}=\sum_{n=0}^\infty\frac{\Delta(k)^n}{[\eta_{s1}^+(k)]^{n+1}}. \tag{67}$$

The expansion is possible since

$$\eta_{s1}^+(k)=k-\omega_1-2\int_0^\infty dk'\,\mathrm{P}\left(\frac{\lambda^2 v_{k'}^2(1+\cos k'x_{21})}{k-k'}\right)$$
$$+2\pi\lambda^2 v_k^2\sin kx_{21}+2\pi i\lambda^2 v_k^2, \tag{68}$$

$$|\Delta(k)|=|\mathrm{Im}[\eta_{s1}^+(k)]|\leqslant|[\eta_{s1}^+(k)]|. \tag{69}$$

Using Eq. (67), Eq. (61) is written as

$$\mathcal{A}(t)=\frac{1}{2\pi i}\int_0^\infty dk\frac{e^{-ikt}}{\eta_s^-(k)}$$
$$-\frac{1}{2\pi i}\sum_{n=0}^\infty\int_0^\infty dk\frac{(-2\pi i\lambda^2 v_k^2)^n e^{-ik(t-nx_{21})}}{[\eta_{s1}^+(k)]^{n+1}}. \tag{70}$$

In Eq. (70), the pole contributions come from $1/[\eta_{s1}^+(k)]^{n+1}$. For $n=0$, $e^{-ikt}/\eta_{s1}^+(k)$ has a simple pole in the lower half plane at $k=z_{s1}$. Its effect appears for $t>0$, when we can close the integration contour in the lower half plane. For $n=1$, $e^{-ik(t-x_{21})}/[\eta_{s1}^+(k)]^2$ has a double pole. Its effect appears for $t>x_{21}$. In general, for each x_{21} time step there appears a new pole effect which is smaller by order λ^2 than the previous pole effect. In this way we can explain the wiggling decay rate (Fig. 2).

As we discuss now, this description of the bounces is connected to emergence of the collective state. Approximating (for $\lambda\ll 1$)

$$\eta_{s1}^+(k)\approx k-z_{s1}, \tag{71}$$

the pole contributions in Eq. (70) are given by

$$\mathcal{A}_0(t)\equiv\frac{-1}{2\pi i}\int_{-\infty}^\infty dk\frac{1}{k-z_{s1}-\Delta(k)}e^{-ikt}$$
$$=\frac{-1}{2\pi i}\sum_{n=0}^\infty\int_{-\infty}^\infty dk\frac{\Delta(k)^n}{(k-z_{s1})^{n+1}}e^{-ikt}. \tag{72}$$

Taking the residues at the pole $k=z_{s1}$ we obtain an expression of the piecewise form

$$\mathcal{A}_0(t) = \sum_{n=0}^{\infty} \theta(t - nx_{21}) g_n(t), \tag{73}$$

where

$$g_n(t) = -\left[\frac{1}{n!} \frac{\partial^n}{\partial k^n} \Delta(k)^n e^{-ikt} \right]_{k=z_{s1}}. \tag{74}$$

We have $g_n \sim \lambda^{2n}$. Note that the sum stops at n such that $t < nx_{21}$. Since for weak coupling the terms $g_n(t)$ become smaller as n increases, after a few bounces we have

$$\mathcal{A}_0(t) \approx \tilde{\mathcal{A}}_0(t), \tag{75}$$

where

$$\tilde{\mathcal{A}}_0(t) = \sum_{n=0}^{\infty} g_n(t). \tag{76}$$

As shown in Appendix A we have

$$\tilde{\mathcal{A}}_0(t) = N_s e^{-iz_s t} \tag{77}$$

for all $t > 0$, where

$$N_s = \left. \frac{1}{1 - \partial\Delta(k)/\partial k} \right|_{k=z_s} \tag{78}$$

for weak coupling. Equation (77) shows that the sum of all bounces gives the contribution from the collective state $|\phi_s\rangle$ with eigenvalue z_s.

Equation (77) is consistent with z_s giving the slowest exponential decay. To see this we use Eq. (62) to write the equation for $z_{s,n}$ as

$$\eta_{s1}^{+}(z_{s,n}) - \Delta(z_{s,n}) = 0 \tag{79}$$

or

$$z_{s,n} \approx z_{s1} + \Delta(z_{s,n}) \tag{80}$$

[for $x_{21} \gg \omega_1^{-1}$ we have $z_{s1} \approx z_1$ and we recover Eqs. (38) and (39) for $j = s$].

The function $k - z_{s1} - \Delta(k)$ in Eq. (72) has zeros at $k = z_{s,n}$. For $t \to \infty$ only the residue at the pole $k = z_{s,0} = z_s$ remains, and we get

$$\lim_{t\to\infty} N_s^{-1} e^{iz_s t} \mathcal{A}_0(t) = \lim_{t\to\infty} N_s^{-1} e^{iz_s t} \tilde{\mathcal{A}}_0(t) = 1, \tag{81}$$

which is consistent with Eq. (77).

VI. DECAY RATE AND ENERGY VS DISTANCE

In this section we investigate the behavior of the complex eigenvalues of the Hamiltonian z_j for different values of x_{21}.

The equation $\eta_j^{+}(z) = 0$ can be solved numerically by iterations of $z = z - \eta_j^{+}(z)$. The imaginary and real parts of z thus obtained are shown in Figs. 6 and 7 (we used the same parameters as in the previous figures). The numerical iteration was started around $z = \omega_1$ so, with the exception of two isolated points seen in Fig. 6, the solutions obtained are the collective eigenvalues $z = z_j$ and not the poles $z_{j,n}$ of the Green's function. Gaps in the graphs are points missed by the numerical solution.

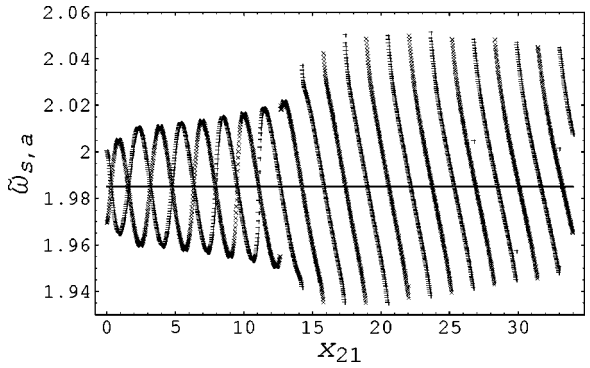

FIG. 7. The energies $\tilde{\omega}_s$ (×) and $\tilde{\omega}_a$ (+) as a function of x_{21}. They oscillate with x_{21}. The solid line is the one-atom energy $\tilde{\omega}_1 = 1.985$. Both x_{21} and $\tilde{\omega}_{s,a}$ are dimensionless.

As we see, γ_j and $\tilde{\omega}_j$ oscillate with x_{21}. The oscillation period is approximately $2\pi/\tilde{\omega}_1$ where $\tilde{\omega}_1$ is the one-atom renormalized frequency (see Appendix B).

Due to the oscillations, the collective decay rate can become smaller or larger than the one-atom decay rate (solid line in Fig. 6). We have subradiance and superradiance, respectively. In particular, it is noticeable that there are distances at which the decay rates γ_j vanish (see Appendix B). This means that for these distances there is no outgoing radiation. The outgoing emitted fields of the atoms cancel by destructive interference and a standing field is trapped between the two atoms, storing energy. Note that both symmetric and antisymmetric initial conditions can give rise to either subradiant or superradiant states, since both γ_s and γ_a oscillate with x_{21}.

The oscillations of the decay rate and the energy shown in Figs. 6 and 7 are a unique feature of one-dimensional systems. For two or three dimensions, these quantities can change significantly only for short distances between atoms (see Appendix C).

As an example of subradiance and superradiance we show numerical simulations with the same parameters used in the previous examples, except we choose $L = 250$ (to have higher space resolution) and $x_{21} = 12.7$. For this value of x_{21}, the decay rate of the antisymmetric state vanishes while the decay rate of the symmetric state is maximum (see Fig. 6). In Fig. 8 we show the survival probability of atom 1 for antisymmetric and symmetric initial conditions, showing the appearance of stationary subradiant collective state and a superradiant collective state. In Figs. 9 and 10 we show the corresponding fields.

We turn to the force between the atoms. Here we will give only a heuristic discussion. A more detailed analysis requires including the Casimir-Polder or van der Waals forces between the atoms, as well as the inertia of the atoms, which we are not considering in this paper.

Since the atoms are unstable, the force between them should be time dependent [23]. We expect the force to decay exponentially during the time scales where the collective-state components dominate. For the dependence on x_{21} of the force, the quantity

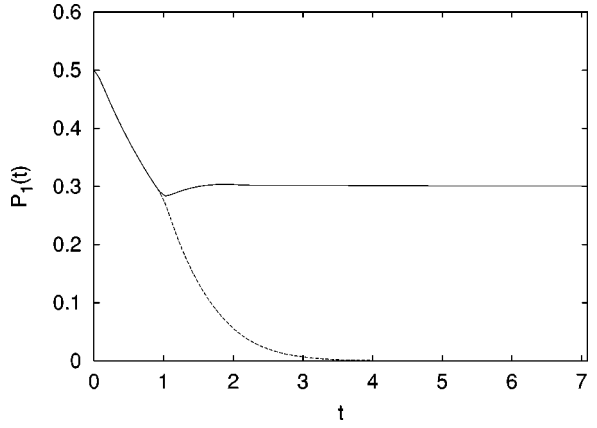

FIG. 8. Survival probability $P_1(t)$ of atom 1 for antisymmetric initial condition (solid) giving rise to a subradiant stationary collective state, and symmetric initial condition (dashed) giving rise to a superradiant collective state. Before $t=x_{21}$, $P_1(t)$ has the one-atom decay rate. Time t has been scaled to units of $x_{21}=12.7$.

$$\mathcal{F}_j = -\, d\tilde{\omega}_j/dx_{21} \tag{82}$$

can give an indication because $\tilde{\omega}_j$ is the average energy of the collective state.

As we can see in Fig. 11, $\mathcal{F}_s$ oscillates with x_{21} ($\mathcal{F}_a$ has a similar behavior). $\mathcal{F}_s>0$ corresponds to a repulsive force, and $\mathcal{F}_s<0$ to an attractive force. Attraction is strongest ($\mathcal{F}_s$ is locally a minimum) when the collective decay rate is largest ($-\gamma_s$ is locally a minimum as well). The atoms tend to attract each other when they emit the field outward and tend to repel when the field remains trapped between them.

We also see in Fig. 11 that there are points x_{21}^0 for which $\mathcal{F}_s$ vanishes. If $d\mathcal{F}_s/dx_{21}<0$ at these points, then any small displacement Δx_{21} around x_{21}^0 creates a force in the opposite direction. Thus in this case x_{21}^0 are stable points (if $d\mathcal{F}_s/dx_{21}>0$ the points are unstable). The existence of stable

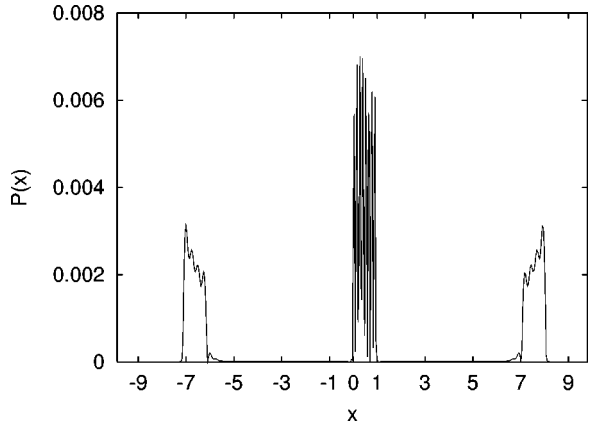

FIG. 9. Field intensity $P(x,t)$ for the atoms in a stationary collective state. Space coordinate x is in units of $x_{21}=12.7$ and $P(x,t)$ is dimensionless. The field between the two atoms located at $x=0$ and $x=1$ remains trapped. The initial condition is $|a\rangle$. Time is $t=7.09x_{21}$. The wave packets on each side move outward with the speed of light $c=1$. They were emitted before the atoms formed the collective state. After that, emission stopped.

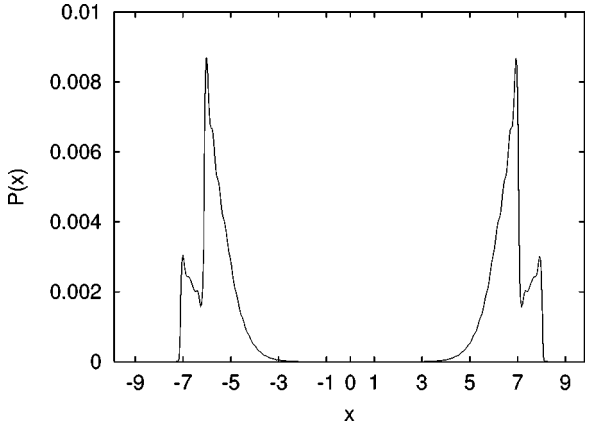

FIG. 10. Field intensity $P(x,t)$ for initial condition $|s\rangle$ at time $t=7.09x_{21}$. Space coordinate x is in units of $x_{21}=12.7$ and $P(x,t)$ is dimensionless. The collective state has decayed. The smaller peaks on the far sides are the field emitted individually by each atom before attaining the collective state. The larger peaks correspond to the two-atom collective emission (superradiance).

points suggests the possibility of having a one-dimensional "molecule." This molecule would have a lifetime of the order of γ_s^{-1}.

VII. TWO-CAVITY WAVEGUIDES

So far, we discussed various properties of collective decay states for the one-dimensional two-atom model which is exactly solvable. Not only is it theoretically simple, this model has another practical advantage since some systems can be mapped into similar form. After the mapping is done, we can see in different systems the same properties we discussed before.

One specific example is a two-cavity electron waveguide (Fig. 12). As shown in Refs. [17,18], the two-cavity waveguide Hamiltonian can be mapped into the same form as Eq. (20), and the same properties we discussed above can be found. Here we present the main ideas. More details will be given in a subsequent paper [24].

The waveguide can be constructed by superposing two closed identical cavities and a lead in two-dimensional space. When we consider the cavities and the lead separately, this

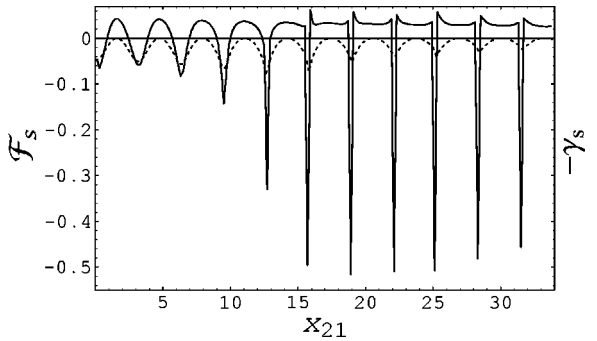

FIG. 11. Graph of $\mathcal{F}_s=-d\tilde{\omega}_s/dx_{21}$ (black line) and the decay rate $-\gamma_s$ (dotted line). We see that when $-\gamma_s$ is a local minimum $\mathcal{F}_s$ also has a local minimum value. All variables are dimensionless.

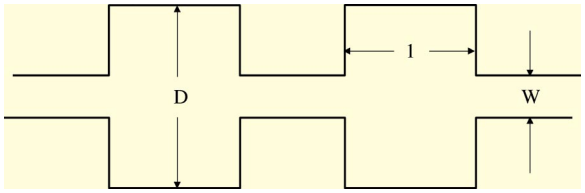

FIG. 12. A two-cavity waveguide.

forms an unperturbed system. The interaction appears as the cavities and the lead are connected.

In suitable units the horizontal dimension of the cavities is 1, and the vertical dimension is D. The lead has a horizontal dimension $L\rightarrow\infty$ and a vertical dimension W. We consider a nonrelativistic electron, neglecting the spin.

If the electron is placed inside a closed cavity, its wave functions correspond to discrete cavity modes. The cavity modes can be labeled as $|m,n\rangle$, where m,n are positive integers representing the horizontal and vertical wave numbers. The corresponding energies are

$$\xi^{m,n} = m^2 + n^2/D^2. \tag{83}$$

An electron placed inside the lead (with no cavities) has modes that can be labeled as $|k,l\rangle$ where kL/π is the horizontal wave number and l the vertical wave number. The energies are

$$E_{k,l} = k^2/\pi^2 + l^2/W^2. \tag{84}$$

As $L\rightarrow\infty$, k becomes a continuous variable. On the other hand, m, n, and l are always positive integers.

We consider an electron with low energy narrowly centered around

$$\xi^0 = \xi^{m_0,n_0}. \tag{85}$$

We assume that

$$E_{0,1} < \xi^0 < E_{k,l} \tag{86}$$

for $l>1$ and all k. The electron may propagate through the first mode of the lead, but not through the $l>1$ modes.

We also assume that there are no other cavity modes with energy between $E_{0,1}$ and ξ^0. Under these conditions, the cavity mode ξ^0 behaves essentially like the excited state in the Friedrichs-Lee model. It will decay with a finite lifetime. This means that an electron inside the cavity will escape through the lead.

The following approximate Hamiltonian is obtained [18]:

$$H_{WG} = \xi^0[|1\rangle\langle 1| + |2\rangle\langle 2|] + \int_0^\infty dk \sum_{l=1}^\infty E_{k,l}|\psi_{k,l}\rangle\langle\psi_{k,l}| + \left(\int_0^\infty dk \sum_{l=1}^\infty V_1(k,l)|1\rangle\langle\psi_{k,l}| + V_2(k,l)|2\rangle\langle\psi_{k,l}| + \text{H.c.}\right). \tag{87}$$

Here, H.c. means Hermitian conjugate. The cavities are centered at $x=x_1$ and $x=x_2$, where x is the horizontal coordinate. The states $|i\rangle$ represent the electron inside cavity $i=1$ or 2, occupying the mode ξ^0. The states $|\psi_{k,l}\rangle$ are modified lead modes; they essentially represent the electron inside the part of the lead that does not overlap with the cavities. The terms $V_i(k,l)$ represent the amplitude of a transition of the electron from this part of the lead to the cavities, or vice versa. Their detailed expression is given in Refs. [18,24]. Here we note only that they have the forms

$$V_1(k,l) = V(k,l,x_1,x_2)e^{ikx_1},$$

$$V_2(k,l) = V(k,l,x_2,x_1)e^{ikx_2}. \tag{88}$$

The Hamiltonian H_{WG} has the same form as our two-atom Friedrichs-Lee model Hamiltonian. As the two cavities are identical, we have a system analogous to the two identical atoms. Since there is only one continuous variable k describing the propagation along the lead, we can think of the waveguide system as a one-dimensional system, with internal degree of freedom l (note that l is discrete).

Similar to the results of Sec. III we obtain the equation for the complex energy of the collective state

$$z_j^0 = \xi^0 + 2\int_0^\infty dk \sum_{l=1}^\infty \frac{|f_j(k,l)|^2}{(z_j^0 - E_{k,l})^+}(1+\sigma_j \cos kx_{21}), \tag{89}$$

where $f_j(k,l)$ is a function of $V_1(k,l)$ and $V_2(k,l)$. We will show that there is a solution with vanishing decay rate, corresponding to a stable collective state. We follow the procedure shown in Appendix B. For a vanishing decay rate we write $z_j^0 = \tilde{\xi}_j^0 - i\epsilon$, where $\epsilon>0$ is infinitesimal. This gives the following condition on x_{21}:

$$1 + \sigma_j \cos k_0 x_{21} = 0, \tag{90}$$

where k_0 is a wave vector that satisfies

$$E_{k_0,l} = \tilde{\xi}_j^0, \quad l=1. \tag{91}$$

Through these two equations, x_{21} for the vanishing decay rate becomes a function of $\tilde{\xi}_j^0$,

$$x_{21} = g(\tilde{\xi}_j^0) \equiv \frac{n}{\sqrt{\tilde{\xi}_j^0 - E_{0,1}}}, \tag{92}$$

where n is an odd integer for $j=s$ and an even integer for $j=a$. The renormalized energy $\tilde{\xi}_j^0$ is given by solution of the integral equation

$$\tilde{\xi}_j^0 = \xi_0 + 2\int_0^\infty dk \sum_{l=1}^\infty |f_j(k,l)|^2 \mathrm{P}\frac{1}{\tilde{\xi}_j^0 - E_{k,l}}\{1+\sigma_j \cos[kg(\tilde{\xi}_j^0)]\}, \tag{93}$$

where P means the principal part. Similar to Eq. (B11), this equation has a solution if the condition

$$\xi^0 - E_{0,1} > 2\int_0^\infty dk \sum_{l=1}^\infty |f_j(k,l)|^2 \mathrm{P}\frac{1}{E_{k,l} - E_{0,l}} \tag{94}$$

is satisfied. If the interaction between each cavity and the lead is small, we can replace $f_j(k,l)$ by the interaction in a single-cavity system. Then, Eq. (94) is essentially the condition that the electron in a single cavity waveguide has

enough energy ξ^0 to escape through the lead. This condition is analogous to Eq. (7).

In summary, by adjusting the distance between the cavities [so that Eq. (92) is satisfied] we obtain a collective stable state where the electron remains trapped inside the two cavities, in either a symmetric or an antisymmetric state. The electron is trapped even though it would escape if there was only one cavity.

To obtain this result we neglected the influence of cavity modes other than ξ^0. The description of the system improves as more cavity modes are included [18].

The existence of stable configurations in the waveguide could be verified by other methods, including numerical simulations calculating the S matrix, or experiments.

VIII. CONCLUDING REMARKS

We have analyzed a one-dimensional two-atom system using complex collective eigenstates of the Hamiltonian. We found that, in contrast to 3D systems, in 1D collective effects persist for large separations between the atoms. The collective symmetric and antisymmetric states are not limited to the near zone and remain appropriate for large separations (far zone).

The collective effects we described, such as the oscillations of the collective decay rates, have a physical realization in mesoscopic analogs of atomic systems, such as electron waveguides. Models of 1D atoms and waveguides with cavities are quite similar, as they describe discrete energy levels coupled to a continuum [18].

Our method is based on an analysis of the complex poles of the Green's function. One advantage of this method is that it directly gives the collective decay rate of the survival probability, as well as the collective field between the atoms, which emerges as the atoms exchange real photons.

In the present paper we focused on real photons and neglected virtual processes (such as virtual photon exchange when both atoms are excited). In the waveguide problem, virtual processes do not exist. Hence, as long as we focus on waveguides, we need not include these processes. On the other hand, for two-atom systems, these processes do exist and they give a correction to the energy shift and the decay rate of the excited states. For weak atom-field coupling this is a small correction, which nevertheless is worthwhile to consider. This will be done in a subsequent paper.

Emitted photons are described by an exponentially growing field, truncated at the light cone of the atoms. This field plays an important role in the two-atom system, giving a strong influence on the lifetime or average energy of the collective states. This field is directly related to the exponential decay of unstable states, which can be regarded as one of the simplest dissipative phenomena on a microscopic scale. So, in a sense, the formation of collective states is a microscopic nonequilibrium process, driven by dissipation.

ACKNOWLEDGMENTS

We thank Professor R. Passante, Professor T. Petrosky, Professor L. Reichl, and Professor W. Schieve, as well as Dr. G. Akguc, R. Barbosa, Dr. E. Karpov, Dr. C. B. Li, A. Shaji, and M. Snyder for helpful comments and suggestions. We acknowledge the International Solvay Institutes for Physics and Chemistry, the Engineering Research Program of the Office of Basic Energy Sciences at the U.S. Department of Energy, Grant No. DE-FG03-94ER14465, the Robert A. Welch Foundation, Grant No. F-0365, and the European Commission, Project No. HPHA-CT-2001-40002, for supporting this work.

APPENDIX A: PROOF OF EQ. (77)

We start with the expression [see Eq. (76)]

$$\tilde{\mathcal{A}}_0(t) = \frac{1}{2\pi i}\sum_{n=0}^{\infty}\int_C dk \frac{\Delta(k)^n}{(k-z_{s1})^{n+1}} e^{-ikt}, \tag{A1}$$

where C is a clockwise contour surrounding $k=z_{s1}$. Taking the residues at this point we get

$$\tilde{\mathcal{A}}_0(t) = \sum_{n=0}^{\infty}\frac{-1}{n!}\frac{\partial^n}{\partial k^n}[\Delta(k)^n e^{-ikt}]_{k=z_{s1}}. \tag{A2}$$

This is a perturbation expansion around z_{s1}, so it will correspond to the contribution from only the pole z_s and not the poles $z_{s,n}$.

We will show that

$$\frac{\partial}{\partial t}\tilde{\mathcal{A}}_0(t) = -iz_s\tilde{\mathcal{A}}_0(t). \tag{A3}$$

Together with Eq. (81) this will prove Eq. (77). Starting with Eq. (A2) and using

$$\frac{\partial^n}{\partial k^n}AB = \sum_{l=0}^{n}\frac{n!}{l!(n-l)!}\left[\frac{\partial^{n-l}}{\partial k^{n-l}}A\right]\left[\frac{\partial^l}{\partial k^l}B\right], \tag{A4}$$

we obtain

$$\frac{\partial}{\partial t}\tilde{\mathcal{A}}_0(t) = -iz_{s1}\tilde{\mathcal{A}}_0(t) - i\tilde{\mathcal{A}}_1(t), \tag{A5}$$

where

$$\tilde{\mathcal{A}}_m(t) = \sum_{n=0}^{\infty}\frac{-1}{n!}\frac{\partial^n}{\partial k^n}[\Delta(k)^{n+m}e^{-ikt}]_{k=z_{s1}}. \tag{A6}$$

Using Eq. (A4) again we get

$$\tilde{\mathcal{A}}_m(t) = \sum_{l=0}^{\infty}\frac{1}{l!}\tilde{\mathcal{A}}_l(t)\frac{\partial^l}{\partial k^l}[\Delta(k)^m]_{k=z_{s1}}. \tag{A7}$$

With Eq. (80) for $z_{s,0}=z_s\approx z_{s1}+\Delta(z_s)$ and the Taylor expansion of $\Delta(z_s)^l$ around z_{s1} we find that the solution of this system of equations is

$$\tilde{\mathcal{A}}_l(t) = \Delta(z_s)^l\tilde{\mathcal{A}}_0(t), \tag{A8}$$

which combined with Eq. (A5) proves Eq. (A3).

APPENDIX B: OSCILLATIONS OF γ_j AND ω_j WITH x_{21}

In this appendix we will show that the decay rates γ_j and energies $\tilde{\omega}_j$ of the collective states $|\phi_j\rangle$ oscillate with the

distance x_{21} between the atoms. First we will show that γ_s vanishes (comes infinitesimally close to zero) for distances

$$[x_{21}]_{\gamma_s=0} = \frac{(2n+1)\pi}{\tilde{\omega}_s^o}, \tag{B1}$$

where n is an integer, and

$$\tilde{\omega}_s^o = [\tilde{\omega}_s]_{\gamma_s=0}. \tag{B2}$$

Similarly we will show that the decay rate γ_a vanishes for

$$[x_{21}]_{\gamma_a=0} = \frac{2n\pi}{\tilde{\omega}_a^o}, \tag{B3}$$

where

$$\tilde{\omega}_a^o = [\tilde{\omega}_a]_{\gamma_a=0}. \tag{B4}$$

We start with the equation $\eta_s^+(z_s)=0$ or

$$z_s = \omega_1 + 2\int_0^\infty dk \frac{\lambda^2 v_k^2}{(z_s-k)^+}(1+\cos kx_{21}). \tag{B5}$$

Assuming $z_s = \tilde{\omega}_s^o - i\epsilon$ with infinitesimal ϵ we have

$$\begin{aligned}\tilde{\omega}_s^o &= \omega_1 + 2\int_0^\infty dk \frac{\lambda^2 v_k^2}{\tilde{\omega}_s^o - k + i\epsilon}(1+\cos kx_{21}) \\ &= \omega_1 + 2\int_0^\infty dk \lambda^2 v_k^2 \left[\mathrm{P}\frac{1}{\tilde{\omega}_s^o - k} - \pi i \delta(\tilde{\omega}_s^o - k)\right] \\ &\quad \times (1+\cos kx_{21}),\end{aligned} \tag{B6}$$

where we used the relation

$$\frac{1}{\omega + i\epsilon} = \mathrm{P}\frac{1}{\omega} - \pi i \delta(\omega) \tag{B7}$$

together with Eq. (12). Comparing the left- and right-hand sides of Eq. (B6) we see that the imaginary part should vanish, so we get

$$1 + \cos \tilde{\omega}_s^o x_{21} = 0, \tag{B8}$$

which proves Eq. (B1). In a similar way, starting from the equation for z_a,

$$z_a = \omega_1 + 2\int_0^\infty dk \frac{\lambda^2 v_k^2}{(z_a-k)^+}(1-\cos kx_{21}), \tag{B9}$$

we get

$$1 - \cos \tilde{\omega}_a^o x_{21} = 0, \tag{B10}$$

which proves Eq. (B3).

The $\tilde{\omega}_j^o$ satisfy the integral equations

$$\tilde{\omega}_s^o = \omega_1 + 2\int_0^\infty dk \lambda^2 v_k^2 \mathrm{P}\frac{1}{\tilde{\omega}_s^o - k}\left[1 + \cos\frac{(2n+1)\pi k}{\tilde{\omega}_s^o}\right],$$

$$\tilde{\omega}_a^o = \omega_1 + 2\int_0^\infty dk \lambda^2 v_k^2 \mathrm{P}\frac{1}{\tilde{\omega}_a^o - k}\left[1 - \cos\frac{2n\pi k}{\tilde{\omega}_a^o}\right]. \tag{B11}$$

Using graphical methods it can be shown the first equation has a unique solution for each integer n, provided that

$$\omega_1 - 2\lim_{\tilde{\omega}_s^o \to 0}\int_0^\infty dk \lambda^2 v_k^2 \mathrm{P}\frac{1}{k}\left[1 + \cos\frac{(2n+1)\pi k}{\tilde{\omega}_s^o}\right] > 0. \tag{B12}$$

In the limit $\tilde{\omega}_s^o \to 0$ the cosine term gives a vanishing integration. Thus Eq. (B12) is satisfied if Eq. (7) is satisfied. A similar argument applies to the second equation in (B11).

Equations (B1) and (B3) explain the oscillatory behavior of γ_j seen in Fig. 6.

To explain the oscillations of $\tilde{\omega}_j$ we note that the terms inside brackets in Eq. (B11) are even in k around $\tilde{\omega}_j^o$, regardless of n. On the other hand, the principal parts are odd. Hence the product is odd and the integration around $\tilde{\omega}_j^o$ vanishes. Thus the largest contributions to the integrals come from the tails of the principal parts. The "1" terms inside the brackets give a much larger contribution than the "cos" terms, because the latter oscillate with k. Neglecting the "cos" terms, we get

$$\tilde{\omega}_s^o \approx \tilde{\omega}_a^o \approx \tilde{\omega}_1, \tag{B13}$$

where $\tilde{\omega}_1$ is the one-atom shifted energy [see Eq. (14)]. This shows that the $\tilde{\omega}_j$ have approximately the same values when their respective γ_j vanish. From Eq. (B13) we conclude that the period of the oscillations of γ_j and $\tilde{\omega}_j$ is approximately $2\pi/\tilde{\omega}_1$.

Adding Eqs. (B5) and (B9) we see that for weak coupling the poles of the one- and two-atom Green's functions obey the relations

$$z_1 \approx \frac{z_a + z_s}{2}. \tag{B14}$$

So both $\tilde{\omega}_j$ and γ_j oscillate around the one-atom $\tilde{\omega}_1$ and γ_1, respectively.

Finally, we show that the "force" $\mathcal{F}_s$ between the atoms is a local maximum when the decay rate is zero, as seen in Fig. 11. When $\gamma_s=0$, we have

$$\frac{d\mathcal{F}_s^0}{dx_{21}} = -\frac{d^2\tilde{\omega}_s^o}{dx_{21}^2} \approx 2\int_0^\infty dk \lambda^2 v_k^2 \mathrm{P}\frac{1}{\tilde{\omega}_s^o - k}k^2 \cos\frac{(2n+1)\pi k}{\tilde{\omega}_s^o}. \tag{B15}$$

As argued above Eq. (B13) the integral of the cosine is small. Hence we have

$$\frac{d\mathcal{F}_s^o}{dx_{21}} \approx 0. \tag{B16}$$

A similar argument may be applied to $\mathcal{F}_a$.

APPENDIX C: SUBRADIANCE IN $d>1$ DIMENSIONS

In one dimension, the vanishing of the collective decay rate occurs for distances given by the conditions

$$1 + \sigma_j \cos \tilde{\omega}_j^o x_{21} = 0. \tag{C1}$$

Assuming the potential v_k is rotationally invariant, in $d>1$ dimensions, analogous conditions would be

$$\int_0^\pi \Omega(\theta) d\theta [1 + \sigma_j \cos(\tilde{\omega}_j^o x_{21} \cos \theta)] = 0, \tag{C2}$$

where θ is the angle of the wave vector $\mathbf{k}$ with respect to the line joining the two atoms. The function Ω is 2 for $d=2$ and $\sin \theta$ for $d=3$.

We see that Eq. (C2) can be satisfied only for the antisymmetric state with $\sigma_j=-1$ and for short distances $x_{21} \ll [\tilde{\omega}_j^o]^{-1} \approx \tilde{\omega}_1^{-1}$. This agrees with the results of Stephen [4] anticipated by Dicke [1].

[1] R. H. Dicke, Phys. Rev. **93**, 99 (1954).
[2] W. Woger, H. King, R. Glauber, and J. H. Haus, Phys. Rev. A **34**, 4859 (1986).
[3] C. Compgano, G. M. Palma, R. Passante, and F. Persico, J. Phys. B **28**, 1105 (1995).
[4] M. J. Stephen, J. Chem. Phys. **50**, 669 (1964).
[5] P. W. Milonni and P. L. Knight, Phys. Rev. A **10**, 1096 (1974).
[6] H. T. Dung and K. Ujihara, Phys. Rev. A **59**, 2524 (1999).
[7] E. A. Power and T. Thirunamachandran, Phys. Rev. A **51**, 3660 (1995); **47**, 2539 (1993).
[8] H. T. Dung and K. Ujihara, Phys. Rev. Lett. **84**, 254 (2000).
[9] G. I. Kweon and N. M. Lawandy, Phys. Rev. A **47**, 4513 (1993); **49**, 2205 (1994).
[10] Z. Ficek, Phys. Rev. A **44**, 7759 (1991).
[11] T. Petrosky, G. Ordonez, and I. Prigogine, Phys. Rev. A **64**, 062101 (2001).
[12] N. Nakanishi, Prog. Theor. Phys. **19**, 607 (1958).
[13] E. C. G. Sudarshan, C. B. Chiu, and V. Gorini, Phys. Rev. D **18**, 2914 (1978).
[14] A. Böhm and M. Gadella, *Dirac Kets, Gamow Vectors and Gelfand Triplets*, *Lecture Notes on Physics*, Vol. 348 (Springer, New York, 1989).
[15] T. Petrosky, I. Prigogine, and S. Tasaki, Physica A **173**, 175 (1991).
[16] S. Kim and G. Ordonez, e-print physics/0311048.
[17] T. Petrosky and S. Subbiah, Physica E (Amsterdam) **19**, 230 (2003).
[18] S. Subbiah, Ph.D. dissertation, The University of Texas at Austin, 2000.
[19] U. Weiss, *Quantum Dissipative Systems* (World Scientific, Singapore, 1993).
[20] P. Facchi and S. Pascazio, Physica A **271**, 133 (1999).
[21] C. Cohen-Tannouji, J. Dupont-Roc, and G. Grynberg, *Atom-Photon Interactions: Basic Processes and Applications* (Wiley, New York, 1992), p. 248.
[22] http://www.netlib.org/eispack/
[23] R. Passante and F. Persico, e-print quant-ph/0212163.
[24] S. Kim, K. Na, and G. Ordonez (unpublished).